

Role of syndrome information on a one-way quantum repeater using teleportation-based error correction

Ryo Namiki,¹ Liang Jiang,² Jungsang Kim,³ and Norbert Lütkenhaus¹

¹*Institute for Quantum Computing and Department of Physics and Astronomy, University of Waterloo, Waterloo, Ontario, Canada N2L 3G1*

²*Department of Applied Physics, Yale University, New Haven, Connecticut 06511, USA*

³*Electrical and Computer Engineering Department, Duke University, Durham, North Carolina 27708, USA*

(Received 3 August 2016; published 3 November 2016)

We investigate a quantum repeater scheme for quantum key distribution based on the work by S. Muralidharan *et al.* [*Phys. Rev. Lett.* **112**, 250501 (2014)]. Our scheme extends that work by making use of error syndrome measurement outcomes available at the repeater stations. We show how to calculate the secret key rates for the case of optimizing the syndrome information, while the known key rate is based on a scenario of coarse graining the syndrome information. We show that these key rates can surpass the Pirandola-Laurenza-Ottaviani-Banchi bound on secret key rates of direct transmission over lossy bosonic channels.

DOI: 10.1103/PhysRevA.94.052304

I. INTRODUCTION

To explore the possibility of quantum communication schemes over a long distance [1–5], an essential question is whether the secret key generation rate of the quantum key distribution (QKD) with the help of intermediate stations could be better than *any* key generation scheme without intermediate stations. A clear criterion for this is to surpass the Takeoka-Guha-Wilde (TGW) bound [6,7]. This is an upper bound of the secret key rate per optical mode over a pure lossy channel and is given by

$$R_{\text{TGW}} = \log_2 \frac{1 + \eta}{1 - \eta}, \quad (1)$$

where $\eta \in (0,1]$ is the transmission of the lossy channel. Hence, any key generation over a distance corresponding to the transmission η cannot surpass R_{TGW} when there are no intermediate stations. While the TGW bound was suggested to be unachievable, Pirandola, Laurenza, Ottaviani, and Banchi (PLOB) have reported that the corresponding tight bound is given by [8,9]

$$R_{\text{PLOB}} = \log_2 \frac{1}{1 - \eta}. \quad (2)$$

It has been shown that the TGW bound cannot be overcome if we are only able to use Gaussian channels as intermediate stations in a one-way structure [10]. This no-go statement for Gaussian repeaters holds also for the PLOB bound. An open question is whether there are other simple intermediate stations facilitating quantum repeater behavior.

Recently, various quantum repeater architectures have been studied [11–14]. Ultimately, one-way schemes with a teleportation-based error-correction (TEC) approach [15,16] have an advantage in terms of achievable rates. Due to the structure of the error correction, the syndrome information of all intermediate stations is available for optimizing the key rate. In Ref. [12], the syndrome measurement was used to flag success or failure events and to reduce the effective errors in the success case. The secret key rate was then analyzed by calculating the probability that all intermediate

stations show success events and by calculating the expected remaining error rates. No further details of the syndrome measurements have been used. Hence, an attainable key rate is immediately determined without the need for keeping track of every combination of possible syndrome outcomes coming through all intermediate stations. This theoretical simplicity also suggests a relatively low technical difficulty for a practical implementation. On the other hand, such a coarse-grained treatment of the syndrome outcomes will discard some of useful information, and the key rate will be lower than potentially achievable performance of a one-way protocol that makes use of the fine-grained syndrome information. In other words, we can obtain a better key rate when we keep the syndrome information and optimize its use. The question is how significant this improvement is, so that one can decide whether it is worthwhile to invest the additional processing overhead required for the fine-grained treatment.

In this paper, we show how to calculate the secret key rate of one-way schemes when the syndrome measurement outcomes are taken into account and address the question of whether they can be potentially useful in overcoming the PLOB bound. We positively answer this question by showing that one can beat the PLOB bound by making an appropriate choice of parameters. We also point out that our intermediate stations are regarded as quantum channels, and there exist simple quantum-channel stations which facilitate the behavior of a quantum repeater. Although a fine-grained treatment of the syndrome outcomes is not necessary to surpass the PLOB bound, it turns out to be useful to extend the transmission distance and improve error tolerance for a high-rate key generation above the PLOB bound.

This paper is organized as follows. After an introduction of the models and related basic notions of one-way stations, we show how to calculate the secret key rate with the use of syndrome information in Sec. II. We compare the key rates for various parameters and identify the area where the performance of the TEC stations surpasses the PLOB bound in Sec. III. There, we also describe the design of a quantum channel station that is sufficient to surpass the PLOB bound. We summarize the results in Sec. IV.

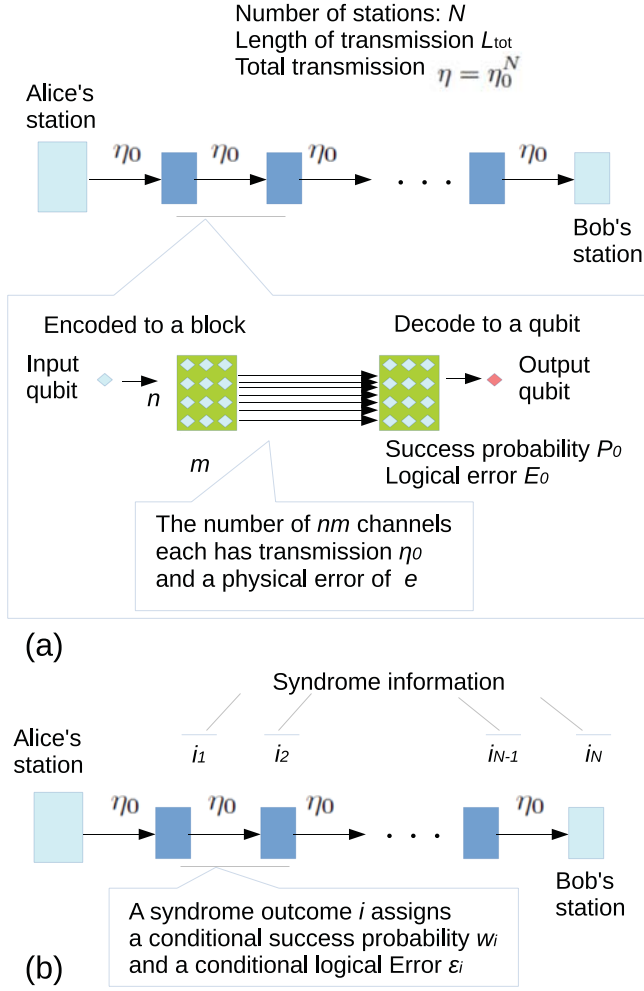


FIG. 1. Encoded transmission of a logical qubit based on a block of $N_p = nm$ single photons (physical qubits). (a) Transmission through a concatenation of intermediate stations. Each station is composed of a decoder and an encoder. A unit segment is connected with the number of nm optical-loss channels whose transmission is η_0 and qubit-error rate is e . The efficiency of the unit segment can be described by the success probability P_0 that the logical qubit is received and the average error E_0 of the successfully received logical qubit. (b) It is not necessary for the intermediate stations to physically execute a decoding operation to output a logical qubit. But an error correction, a syndrome measurement followed by a recovery operation, can be performed effectively by keeping the syndrome information of intermediate stations $\{i_1, i_2, \dots, i_N\}$. A syndrome outcome of a single station i assigns conditional success probability w_i and conditional logical error ϵ_i . The set $\{w_i, \epsilon_i\}$ and the measured sequence $\{i_1, i_2, \dots, i_N\}$ determine the net performance of the transmission.

II. STRUCTURE OF INTERMEDIATE STATIONS AND SECRET KEY RATE

A. One-way stations and basic mechanism

Let us consider transmission of a logical qubit using a set of single-photon polarization qubits with repeater stations that perform quantum error correction as in Fig. 1. Suppose that the error correction works with a success probability P_0 and

gives a logical error rate E_0 (averaged over phase and bit) for a lossy segment of transmission $\eta_0 \in (0, 1)$. A concatenation of N segment and station pairs, consisting of loss segments and repeater station units, has the net success probability

$$P_{\text{succ}} = P_0^N \quad (3)$$

and the net average logical error rate

$$Q_N = \frac{1 - (1 - 2E_0)^N}{2}. \quad (4)$$

Up to a factor of the protocol efficiency $1/2$, the key rate for the Bennett-Brassard 1984 (BB84) protocol with this concatenated transmission is given by [17]

$$K = P_{\text{succ}} \max[\{1 - 2h(Q_N)\}, 0], \quad (5)$$

where $h(x) = -x \log_2 x - (1-x) \log_2 (1-x)$ is the binary entropy function. The net error of Eq. (4) comes from the fact that a link of two binary symmetric channels with the error rates ϵ_1 and ϵ_2 becomes another binary symmetric channel with the error rate

$$G(\epsilon_1, \epsilon_2) := \epsilon_1(1 - \epsilon_2) + \epsilon_2(1 - \epsilon_1). \quad (6)$$

Suppose that the number of photonic qubits transmitted per logical qubit is N_p . Since a polarization qubit uses two modes, the number of modes physically used in this transmission is $2N_p$. This implies that the key rate per mode is given by

$$R = \frac{K}{2N_p}. \quad (7)$$

On the other hand, the key rate due to the direct transmission of a single photon over the pure lossy line with the transmission $\eta = \eta_0^N$ is given by

$$R_d = \frac{1}{2} \max\{\eta[1 - 2h(0)], 0\} = \frac{1}{2} \eta_0^N, \quad (8)$$

where the factor 2 is again due to the number of optical modes. For a long distance $\eta \ll 1$, the PLOB bound also gives the key rate proportional to the overall transmission

$$R_{\text{PLOB}} = \log_2 \frac{1}{1 - \eta} \simeq 1.44\eta = 1.44\eta_0^N. \quad (9)$$

By comparing R_{PLOB} and the expression in Eqs. (7), the transmission with the intermediate stations beats the PLOB bound if the condition $K > 2N_p R_{\text{PLOB}}$ is satisfied. With the help of Eqs. (3) and (5), this condition can be rewritten for a long distance as

$$P_0 > \eta_0 \left(\frac{2.88N_p}{1 - 2h(Q_N)} \right)^{1/N} \quad (10)$$

whenever $1 - 2h(Q_N) > 0$ holds. If the logical error rate is zero, i.e., $Q_N = 0$, we have

$$P_0 > \eta_0 (2.88N_p)^{1/N}. \quad (11)$$

Since the N th root rapidly converges to 1 as N becomes larger, we have a simple relation for $N \rightarrow \infty$:

$$P_0 > \eta_0. \quad (12)$$

Therefore, an essential necessary condition to beat the PLOB bound is that the success probability of the station is larger than the transmission of the associated segment. We can interpret

the success probability as the success of the transmission, and P_0 is regarded as an effective transmission of the channel. Thereby, the main role of the intermediate stations is to boost the effective transmission. Another essential point is that it becomes easier to beat the PLOB bound when more stations are placed along the total transmission line, as seen in Eq. (11). An important model of the transmission line that fulfills $Q_N = 0$ is the pure bosonic lossy channel. In such a case, an efficient loss error correction to fulfill Eq. (12) is sufficient to beat the PLOB bound. Note that N is associated with the total distance of the transmission as

$$L_{\text{tot}} = -L_{\text{att}} \ln \eta = -NL_{\text{att}} \ln \eta_0, \quad (13)$$

where L_{att} is the attenuation length. In all following numerical results we will use

$$L_{\text{att}} = 20 \text{ km}. \quad (14)$$

Note also that essentially the same discussion holds when we replace the PLOB bound in Eq. (2) with the TGW bound in Eq. (1) as it holds, for $\eta \ll 1$, that

$$R_{\text{TGW}} = \log_2 \frac{1+\eta}{1-\eta} \simeq 2.89\eta = 2.89\eta_0^N. \quad (15)$$

B. Error model

Although the loss in the bosonic channel has the dominant impact on the quantum repeater performance, there will also be finite errors associated with controlling matter qubits in the intermediate stations [12]. As an effective error model, we assume that all errors are induced through the channel and the operations in intermediate stations are perfect. For clarity, we assume each physical qubit suffers a physical error e as in Fig. 1(a). The qubit channel is described by

$$\mathcal{E}_{\text{qubit}}(\rho) = (1 - 2e)\rho + eZ\rho Z + eX\rho X. \quad (16)$$

In our simple error model we assume the error rate to be symmetric in the sense that the qubit bit error is $e_z = e$ and

the qubit phase error is also $e_x = e$. A similar analysis can be performed for a depolarizing channel [12].

C. Protocol

We consider the one-way scheme [12] based on a TEC [18,19]. This scheme is designed to transmit a logical qubit, such as $|\psi_L\rangle = \alpha|0_L\rangle + \beta|1_L\rangle$, encoded in the number of $N_p = nm$ photons with

$$|0_L\rangle = \frac{1}{\sqrt{2}}(|+_L\rangle + |-_L\rangle), \quad (17)$$

$$|1_L\rangle = \frac{1}{\sqrt{2}}(|+_L\rangle - |-_L\rangle),$$

and

$$|\pm_L\rangle = \frac{1}{\sqrt{2}}(\underbrace{|00\dots 0\rangle}_{m} \pm |11\dots 1\rangle)^{\otimes n}, \quad (18)$$

where $n, m \geq 2$. The smallest code uses four photons, and the unit photon block for this case is $(n, m) = (2, 2)$. We will use the pair “ (n, m) ” to specify the block size and thus the code.

Each intermediate station performs a process of the TEC as in Fig. 2. First, we perform a quantum nondemolition (QND) measurement for the incoming qubit block R and identify the positions in the block where the photon is lost. Second, we apply controlled-NOT (CNOT) gates between each of the surviving photons and the corresponding photons of block S . The state of the S block is assumed to be prepared maximally entangled with the outgoing qubit block R' , $(|0_L 0_L\rangle_{SR'} + |1_L 1_L\rangle_{SR'})/\sqrt{2}$, before the CNOT application. Third, we perform a physical X measurement on each photon of block R and a physical Z measurement on each photon of block S . We obtain the measurement outcomes $X_{i,j}^R \in \{\pm 1\}$ and $Z_{i,j}^S \in \{\pm 1\}$ with $i \in \{1, 2, \dots, n\}$ and $j \in \{1, 2, \dots, m\}$, while $X_{i,j} = Z_{i,j} = 0$ is assigned if the index (i, j) corresponds to the position of lost photons.

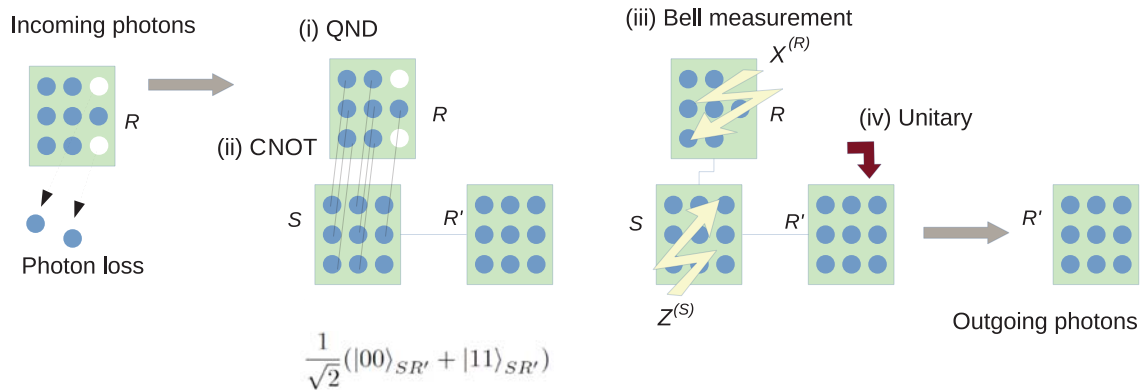


FIG. 2. A quantum-teleportation-based error-correction process transfers the logical qubit of incoming photons in the block R into a fresh logical qubit in the block R' and recovers the photon loss. (i) A quantum nondemolition (QND) measurement of the photon number is performed for each of the physical qubits in R , and the position of the photon loss in the incoming photon block R is identified. (ii) A control-NOT (CNOT) gate is applied between each of the surviving photons in block R and corresponding photons in block S whose logical qubit is prepared to be maximally entangled with the outgoing logical qubit in block R' as $(|00\rangle_{SR'} + |11\rangle_{SR'})/\sqrt{2}$. (iii) A Bell measurement is implemented by logical X and logical Z measurements performed on blocks R and S , respectively. The Pauli operators of logical qubits are decomposed into products of Pauli X and Pauli Z of physical qubits. (iv) Finally, the Pauli frame [16] is adjusted by a unitary operation based on the Bell measurement outcome.

Finally, a unitary operation is performed based on the Bell measurement outcome $(\tilde{M}_X^R, \tilde{M}_Z^S)$ determined by

$$\tilde{M}_X^R = \text{sgn} \left[\sum_{i=1}^n \left(\prod_{j=1}^m X_{i,j}^R \right) \right], \quad (19)$$

$$\tilde{M}_Z^S = \prod_{i=1}^n \left[\text{sgn} \left(\sum_{j=1}^m Z_{i,j}^S \right) \right]. \quad (20)$$

Here, $\text{sgn}(x)$ is associated with the majority vote and assigns $\{-1, 0, 1\}$ depending on $x < 0$, $x = 0$, or $x > 0$, respectively, while the product Π is associated with the parity. If either $\tilde{M}_X^R = 0$ or $\tilde{M}_Z^S = 0$, we say the Bell measurement is inconclusive and discard the transmission attempt through the quantum repeater chain.

We may classify the statistics of the outgoing qubit based on the pattern of the QND outcomes, namely, the number of lost photons and their location. We refer to this information as the pattern component of the syndrome. Let S_{all} be the set of all possible patterns. The performance of the TEC process will be characterized by the syndrome probability $\{w_i\}$ and logical error rates $\{\epsilon_i\}$ associated with the pattern $i \in S_{\text{all}}$. To be specific, we are interested in the joint probability that a recoverable pattern appears and the following Bell measurement is conclusive, i.e., $\tilde{M}_{X,Z} \neq 0$, and the logical error rate of such an event. We may call the subset of the patterns responsible for such events *informative syndromes* S_0 . A detailed note on how to determine this set is presented in the Appendix. As we will see in the next section, the key rate over a sequence of stations is determined by the observed sequence of patterns.

D. Key rate

We will sketch how to calculate the key rate for a sequence of N loss-segment and station pairs whose structure is described in Fig. 1(b). We assume the BB84 protocol corresponding to Sec. II A.

Let $S_0 = \{1, 2, 3, \dots, l\}$ be the set of informative syndromes of a given intermediate station. We denote by $\{w_i\}_{i \in S_0}$ the set of the success probability and by $\{\epsilon_i^{(z)}, \epsilon_i^{(x)}\}_{i \in S_0}$ the associated logical bit error and phase error rates. The total measurement probability and the average error rate over the syndromes S_0 can be associated with P_0 and E_0 in Eqs. (3) and (4) as

$$P_0 = \sum_{i \in S_0} w_i, \quad (21)$$

$$E_0 = \frac{1}{P_0} \sum_{i \in S_0} w_i \left(\frac{\epsilon_i^{(z)} + \epsilon_i^{(x)}}{2} \right).$$

In what follows we may refer to the scenario using these averages as the *coarse-graining* (CG) scenario that discards the index i of informative syndromes. Note that the analysis in Refs. [12, 13] is based on the CG scenario. On the other hand, we may refer to the scenario using all indices of informative syndromes as the *fine-grained* (FG) scenario.

For a sequence of two stations, each transmission of a logical qubit comes with a pair of outcomes i_1 and i_2 . This

formally specifies the process having a set of a probability $w_{i_1, i_2}^{(2)}$ and logical bit and phase errors $\epsilon_{i_1, i_2}^{(2, \gamma)}$ with $\gamma \in \{z, x\}$. Here, 2 in the superscript indicates the number of total stations, and the last station is Bob's station in our notation. By construction we can write

$$w_{i_1, i_2}^{(2)} = w_{i_1} w_{i_2}, \quad (22)$$

$$\epsilon_{i_1, i_2}^{(2, \gamma)} = \epsilon_{i_2, i_1}^{(2, \gamma)} = G(\epsilon_{i_1}^{(\gamma)}, \epsilon_{i_2}^{(\gamma)}),$$

where the function $G(\epsilon_{i_1}, \epsilon_{i_2})$ is given in Eq. (6).

For a sequence of N stations, each transmission of a logical qubit comes with N outcomes i_1, i_2, \dots, i_N , and its statistical property is formally specified by the probability $w_{i_1, i_2, \dots, i_N}^{(N)}$ and logical error rates $\epsilon_{i_1, i_2, \dots, i_N}^{(N, \gamma)}$ with $\gamma \in \{z, x\}$. This implies the following expression for the secure key rate:

$$K = \sum_{i_1, i_2, \dots, i_N} w_{i_1, i_2, \dots, i_N} \times \max \left[0, 1 - \sum_{\gamma \in \{z, x\}} h(\epsilon_{i_1, i_2, \dots, i_N}^{(N, \gamma)}) \right]. \quad (23)$$

For N stations, the number of possible outcomes is l^N . Hence, it seems difficult to calculate the key rate for a large N since the number of relevant terms $\{(w_{i_1, i_2, \dots, i_N}^{(N)}, \epsilon_{i_1, i_2, \dots, i_N}^{(N, z)}, \epsilon_{i_1, i_2, \dots, i_N}^{(N, x)})\}$ increases exponentially with regard to N as $2l^N$. However, as we can see from Eq. (6), the permutation of indices does not change the value of $(w_{i_1, i_2, \dots, i_N}^{(N)}, \epsilon_{i_1, i_2, \dots, i_N}^{(N, z)}, \epsilon_{i_1, i_2, \dots, i_N}^{(N, x)})$. This means that we only need to calculate the triplets whose indices are different under the permutation. By focusing on the number of the same outcomes we can rewrite the key rate of Eq. (23) as

$$K = \sum_{\sum_{i=1}^l N_i = N} w_{\{N_i\}}^{(N)} \max \left[1 - \sum_{\gamma \in \{z, x\}} h(\epsilon_{\{N_i\}}^{(N, \gamma)}), 0 \right], \quad (24)$$

where N_i indicates the number of stations whose measurement outcome is i and

$$w_{\{N_i\}}^{(N)} = \frac{N!}{N_1! N_2! \dots N_l!} \prod_{i=1}^l w_i^{N_i},$$

$$\epsilon_{\{N_i\}}^{(N, \gamma)} = G(\dots G(G(\epsilon_1^{(N_1, \gamma)}, \epsilon_2^{(N_2, \gamma)}), \epsilon_3^{(N_3, \gamma)}), \dots, \epsilon_l^{(N_l, \gamma)})$$

$$= \frac{1}{2} \left(1 - \prod_{i=1}^l (1 - 2\epsilon_i^{(\gamma)})^{N_i} \right), \quad (25)$$

where $\gamma \in \{z, x\}$ and

$$\epsilon_i^{(N_i, \gamma)} = \frac{1 - (1 - 2\epsilon_i^{(\gamma)})^{N_i}}{2}. \quad (26)$$

Now, we can calculate the key rate for an arbitrary N sequence of intermediate stations from the set of the success probability and logical error rates $\{w_i, \epsilon_i^{(z)}, \epsilon_i^{(x)}\}$. A detailed procedure to determine this set for the case of the TEC station with a given set of physical parameters (e, η_0, N) and the code (n, m) is described in the Appendix. In the following numerical calculations, we use a Monte Carlo method to determine the

success probability of the whole sequence of intermediate stations $w_{(N,i)}^{(N)}$ from the set of success probabilities $\{w_i\}_{i \in S_0}$.

III. RESULTS

We will calculate the key rate of the TEC stations based on the formula derived in the previous section and show their potential as a genuine quantum repeater to provide a higher key rate above the PLOB bound.

Our main questions are (i) whether or not the one-way protocol due to the TEC stations can surpass the PLOB bound and (ii) to what extent the syndrome information is significant to boost the key rate. In addition, if the answers are affirmative, we would ask (iii) how small a code could we use and whether the syndrome information helps us to keep the code size smaller. To this end, we will make a comparison between the following three different quantities per channel use for a couple of small-size codes: (a) the fine-grained key rate when retaining all syndrome information, which we refer to as the key rate of the FG scenario R_{FG} , (b) the coarse-grained key rate of the CG scenario R_{CG} , and (c) the PLOB bound R_{PLOB} in Eq. (2). To be specific, as in Eq. (7), we define the FG rate per mode as

$$R_{FG} = \frac{K}{2nm}, \quad (27)$$

with K as defined in Eq. (24). Moreover, we define the key rate per mode for the CG scenario

$$R_{CG} = \frac{P_0^N \max\{[1 - 2h(Q_N)], 0\}}{2nm}, \quad (28)$$

with P_0 and Q_N as defined in Eqs. (4) and (21). This key rate R_{CG} is the rate averaging all informative syndromes.

A. The smallest block encoding (2,2)

Figures 3, 4, and 5 show the typical behavior of the key rates for the smallest code (2,2) with a physical error of $e = 5 \times 10^{-4}$, where the unit transmission is $\eta_0 = 0.97$, $\eta_0 = 0.90$, and $\eta_0 = 0.81$, respectively [on the basis of Eqs. (13) and (14), the unit transmission distance is $L_0 = 0.61, 2.1$, and 4.2 km, respectively). In each of the three graphs, we can observe regimes where R_{FG} beats R_{PLOB} . In Fig. 4 ($\eta_0 = 0.90$) there is also a regime where R_{CG} beats R_{PLOB} , while we do not observe such a regime in Fig. 3 ($\eta_0 = 0.97$) and Fig. 5 ($\eta_0 = 0.81$). Hence, the use of the syndrome information results in a substantial difference in the parametric regime to beat the PLOB bound.

These numerical results positively answer question (i); namely, the one-way protocol with the TEC intermediate stations beats the PLOB bound in a certain parametric regime. Interestingly, even the smallest code of intermediate stations can beat the PLOB bound. Moreover, the CG scenario has a lower key rate than the FG scenario by construction but still has the ability to surpass the PLOB bound. These numerical results also imply that these statements remain essentially the same when we use the TGW bound instead of the PLOB bound. One can see that the TGW bound stays slightly above the PLOB bound in Figs. 3, 4, and 5.

Regarding the second question, we can see from Figs. 3, 4, and 5 that the scenario utilizing the syndrome information

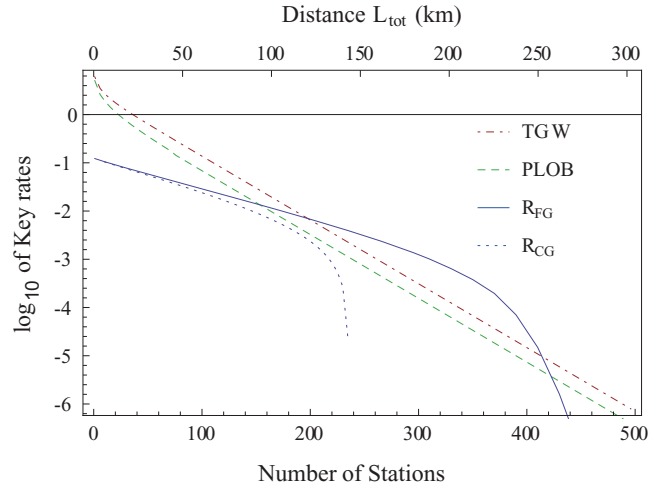


FIG. 3. The key rates ($R_{TGW}, R_{PLOB}, R_{FG}, R_{CG}$) for $\eta_0 = 0.97$ as functions of the number of stations N . At $N \simeq 220$, the key rate of the CG scenario R_{CG} drops rapidly without any crossover to the PLOB bound. For the FG key rate R_{FG} , there is a crossover with the PLOB bound R_{PLOB} . The FG key rate shows relatively slow decay until $N \simeq 400$.

substantially extends the distance where we can find a positive key. Note that the number of stations N is proportional to the distance L_{tot} through the relations in Eqs. (13) and (14). Figure 6 shows an overview of the whole parameter regime where R_{FG} and R_{CG} surpass the PLOB bound in terms of the total distance L_{tot} and the unit transmission η_0 for $e = 5 \times 10^{-4}$. In the shaded area, $R_{FG} > R_{PLOB}$ is satisfied, while inside the dashed loop $R_{CG} > R_{PLOB}$ holds. The distance where the key rate starts to beat the PLOB bound is not very different between R_{FG} and R_{CG} . In contrast, the distance where the key rate falls again below the PLOB bound for the FG scenario is substantially longer than that for the CG scenario. Typically, the additionally gained distance is about 200 km.

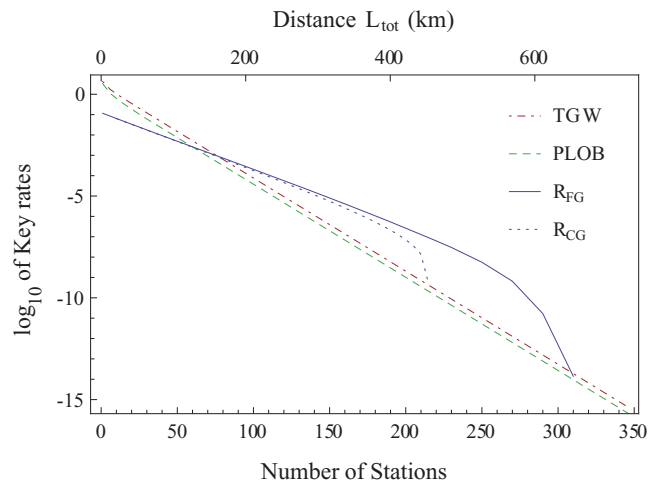


FIG. 4. The key rates ($R_{TGW}, R_{PLOB}, R_{FG}, R_{CG}$) for $\eta_0 = 0.90$ as functions of the number of stations N . For $N \simeq 210$ ($L_{tot} \simeq 440$ km), the CG key rate drops rapidly, whereas the FG key rate holds until $N \simeq 300$ ($L_{tot} \simeq 630$ km).

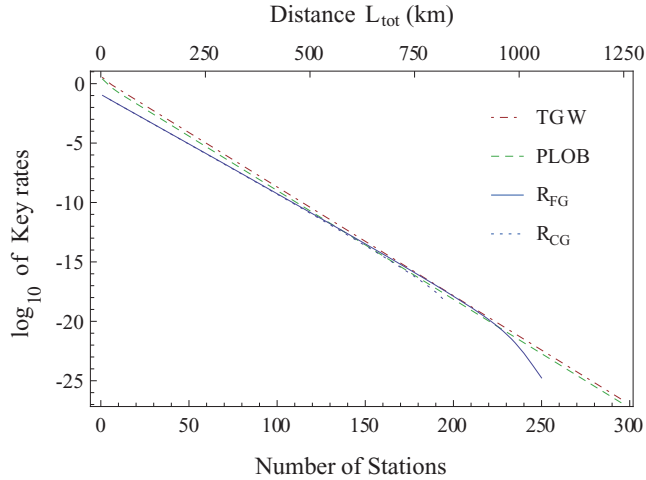


FIG. 5. The key rates (R_{TGW} , R_{PLOB} , R_{FG} , R_{CG}) for $\eta_0 = 0.81$ of the number of stations. The FG key rate R_{FG} marginally goes up to the PLOB bound R_{PLOB} around $N \simeq 190$ (which corresponds to $L_{\text{tot}} \simeq 800$ km), while the CG scenario could not beat the PLOB bound.

It would be worth noting that this specific example of our scheme beats the PLOB bound in a middle distance, such as 200–1000 km, while the key rate of a practical single-photon BB84 protocol using threshold detectors rapidly drops away around 300 km with a moderate dark count rate [17]. Therefore, the code (2,2) provides possible architecture to gain a higher key rate at such a middle distance, although it

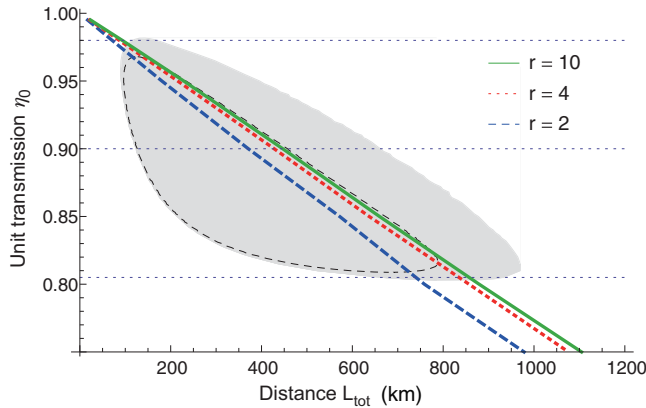


FIG. 6. The gray area shows the regime where the FG key rate surpasses the PLOB bound $R_{\text{FG}} \geq R_{\text{PLOB}}$. The dashed area shows the CG key rate surpasses the PLOB bound $R_{\text{CG}} \geq R_{\text{PLOB}}$. For the dotted level lines $\eta_0 = 0.97$ and $\eta_0 = 0.81$, we can see that the CG key rate R_{CG} cannot surpasses the PLOB bound, while the FG key rate can (see Figs. 3 and 5). On the other hand, the middle of these two level lines shows a wide regime in which both R_{FG} and R_{CG} can surpass the PLOB bound (see the actual behavior of the key rates for the dotted level $\eta_0 = 0.90$ in Fig. 4). Blue dashed, red dotted, and green solid lines show the boundaries where R_{FG} becomes 2, 4, and 10 times larger than R_{CG} , respectively, ($r := R_{\text{FG}}/R_{\text{CG}}$). The code size is $(n, m) = (2, 2)$, and the physical error rate is $e = 5 \times 10^{-4}$. The areas will shrink when the physical error becomes larger (see Fig. 7).

requires a substantial number of stations (~ 200), as shown in Figs. 3, 4, and 5.

In order to view the distinctive role of the syndrome information for gaining a higher key rate over a set of the parameters, we may focus on the ratio between the FG key and the CG key,

$$r = \frac{R_{\text{FG}}}{R_{\text{CG}}}. \quad (29)$$

In Fig. 6, we also show the lines where this ratio r becomes 2, 4, and 10. While a higher value of r does not necessarily mean a substantially higher key rate (because R_{CG} itself may be considerably small), we can ensure a moderate key rate in some cases where we otherwise would not be able to surpass the PLOB bound at all. Figure 6 clearly shows there exists a parameter regime where the following two conditions are simultaneously satisfied: (i) the use of the syndrome information keeps a high key rate which cannot be achieved by any direct transmission, and (ii) it boosts the key rate significantly compared with the key rate of the CG scenario.

For a fixed total distance L_{tot} , we expect a higher number of intermediate stations N would be powerful when there is no physical error. This is because a shorter distance between nearest stations implies a higher success probability. If there is a finite physical error ($e > 0$), a higher number of stations results in a higher total logical error rate because the total logical error accumulates through the action of many stations (recall the unit transmission is η_0 , and the number of stations is the total distance L_{tot} divided by the unit distance $L_0 = -L_{\text{att}} \ln \eta_0$). On the other hand, if we separate the intervals farther from each other, the loss will increasingly reduce the probability of successful photon detection. Hence, given the physical error e and total distance L_{tot} , there is an intermediate optimal value of η_0 to maximize the key rate. In fact, Fig. 6 shows that neither too short a unit distance nor too long a unit distance gives the key rate better than the PLOB bound.

As the physical error rate e increases, it becomes harder to beat the PLOB bound, as illustrated in Fig. 7. The blue outer solid loop and outer dashed loop indicate the regimes $R_{\text{FG}} > R_{\text{PLOB}}$ and $R_{\text{CG}} > R_{\text{PLOB}}$, respectively, for $e = 5.0 \times 10^{-4}$ (the same areas as shown in Fig. 6). Both areas shrink for higher physical errors. The examples shown are the red inner solid loop and the inner dashed loop for $e = 7.5 \times 10^{-4}$. Moreover, for $e = 1.0 \times 10^{-3}$, there is no area to beat the PLOB bound for the CG scenario, while we can observe a small area for the FG scenario. We could not find such an area when $e = 1.5 \times 10^{-3}$ for the FG scenario.

Coupling loss. For practical applications, it is crucial to estimate the effect of the coupling loss. Suppose that every station exhibits the same coupling efficiency η_c for coupling physical qubits into the channel. Then, the coupling loss will modify the unit transmission as $\eta_{\text{eff}} = \eta_c \eta_0$ in the calculation of logical errors while we keep the unit distance $L_0 = -L_{\text{att}} \ln \eta_0$ the same as in Eq. (13). In Fig. 8, we show the area surpassing the PLOB bound for $e = 5.0 \times 10^{-4}$ and $(n, m) = (2, 2)$ with a coupling efficiency of $\eta_c = 0.98$ and $\eta_c = 0.975$, whereas the largest loop is the lossless case. For a 3% coupling loss ($\eta_c = 0.97$) we could not find such an area. Similar behavior can be observed for the case of

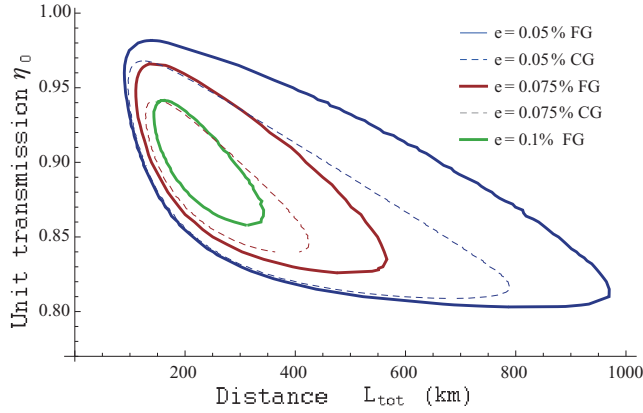


FIG. 7. Areas beating the PLOB bound for the smallest block size $(n,m) = (2,2)$. The two largest areas for the physical error rate $e = 5.0 \times 10^{-4}$ (the ones in Fig. 6) shrink as e becomes higher. For $e = 1.0 \times 10^{-3}$ in the case of the CG scenario R_{CG} , there is no area where the PLOB bound can be beaten, while there still exists a substantial area to beat the PLOB bound for the FG scenario R_{FG} . The right end of the loops for the FG scenario are slightly ragged due to a numerical instability in estimating R_{FG} .

the CG scenario in Fig. 9. The area vanishes when $\eta_c = 0.976$. Consequently, we require a high coupling efficiency $\eta_{\text{eff}} \sim 99\%$ and a lower physical error rate $e \sim 10^{-4}$ so that the one-way scheme with the smallest code $(n,m) = (2,2)$ is experimentally feasible to beat the PLOB bound.

B. Other small-block codes [(3,2), (3,3), (4,3)]

As we have observed in Fig. 7, the physical error rate has to be rather small to beat the PLOB bound via the smallest code (2,2). More specifically, there is almost no hope of beating the PLOB bound for this block size when the physical error rate is $e \geq 1.5 \times 10^{-3}$, even without coupling loss. Fortunately, we can observe better error tolerance for larger block codes.

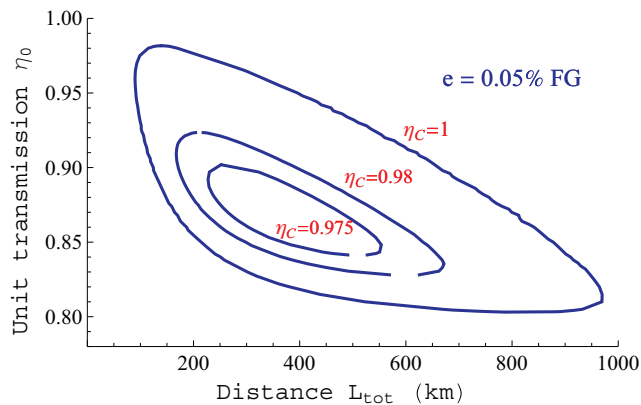


FIG. 8. Areas where the FG key R_{FG} beats the PLOB bound in the presence of a coupling loss for the smallest code $(n,m) = (2,2)$ with a physical error rate of $e = 5 \times 10^{-4}$. The largest loop shows the case without coupling loss ($\eta_c = 1$). The area shrinks with the existence of coupling loss. For a 3% coupling loss ($\eta_c = 0.97$) we could not find the area.

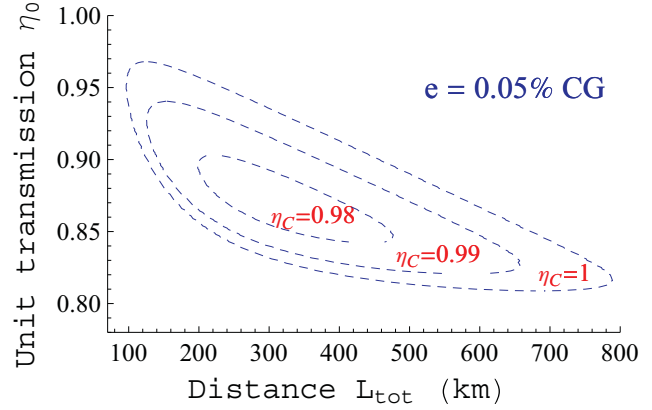


FIG. 9. The areas where the CG key R_{CG} beats the PLOB bound in the presence of a coupling loss for the smallest code $(n,m) = (2,2)$ with a physical error rate of $e = 5 \times 10^{-4}$. The largest loop shows the case without coupling loss ($\eta_c = 1$). The area shrinks due to coupling loss. We could not find the area when the coupling loss is 2.4% ($\eta_c = 0.976$).

The second smallest block size is $(n,m) = (3,2)$. Figure 10 shows the areas that surpass the PLOB bound for a couple of different physical errors e . We can find a substantially wider area to surpass the PLOB bound than with the (2,2) code for both the FG scenario and the CG scenario with $e = 1.0 \times 10^{-3}$ (the green solid middle loop and the green dashed middle loop, respectively). The block size (3,2) also gives a finite area for a larger physical error rate of $e = 1.5 \times 10^{-3}$, while there is no such area when the error rate is $e = 2.0 \times 10^{-3}$. The shape of the areas becomes wider in the vertical direction

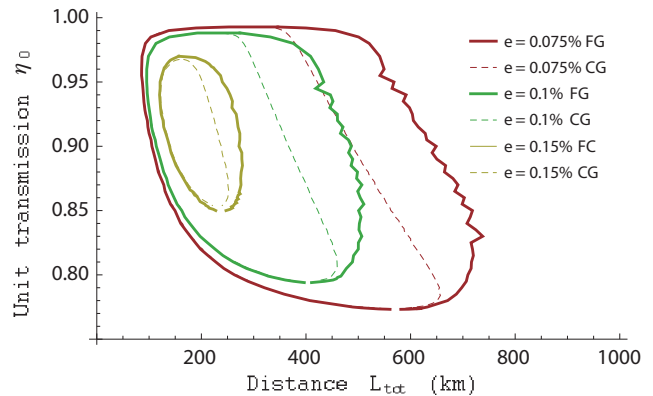


FIG. 10. Areas beating the PLOB bound for a block size of $(n,m) = (3,2)$ with physical error rates of $e = 7.5 \times 10^{-4}$, $e = 1.0 \times 10^{-3}$, and $e = 1.5 \times 10^{-3}$. For this block size, we can observe wider areas to beat the PLOB bound compared with Fig. 7. In particular, we find a relatively wide area for the CG scenario with $e = 1.0 \times 10^{-3}$ beating the PLOB bound (the middle green dashed loop), and there exists such a regime even for a higher error rate of $e = 1.5 \times 10^{-3}$ (the smallest yellow dashed loop). The rightmost boundaries for the FG scenario are jagged due to a numeric instability. Again, for each of the physical error rates, the FG scenario always extends the longest distance to beat the PLOB bound compared with the CG scenario.

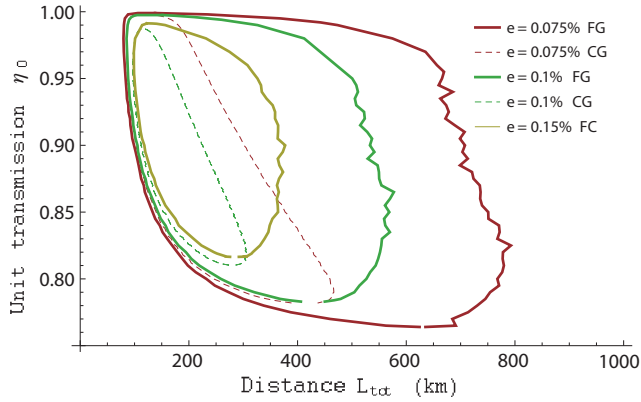


FIG. 11. Areas beating the PLOB bound for a block size of $(n, m) = (3, 3)$. The solid loops are for the FG key rate, and the dashed loops are for the CG rates. The physical error rates are, respectively, $e = 7.5 \times 10^{-4}$, $e = 1.0 \times 10^{-3}$, and $e = 1.5 \times 10^{-3}$ from the largest solid loop to the smallest solid loop for the FG scenario, while there is no area for the CG scenario with $e = 1.5 \times 10^{-3}$. Compared with the block size of $(3, 2)$, the areas for FG key rates grow wider, while the areas for the CG scenario rather shrink. The rightmost boundaries for the FG scenario are jagged due to the numeric instability.

compared with that of the $(2, 2)$ code. This implies that the unit transmission distance between the nearest stations could be larger. Intuitively, the $(3, 2)$ code has a better loss tolerance than the $(2, 2)$ code. This is because the $(2, 2)$ code is unable to maintain the qubit information for the loss of two photons, while the $(3, 2)$ code still has a certain potential for recovering from two photon loss. Note that the right end of the loops for the FG scenario are ragged due to the numerical instability in estimating R_{FG} .

We can observe wider areas for beating the PLOB bound with relatively higher errors by using larger codes. Figure 11 shows the case of the $(3, 3)$ code. In this case, the CG scenario results in smaller areas to beat the PLOB bound when it is compared with the areas for the $(3, 2)$ code of Fig. 10. Notably, the area vanishes when we use the $(3, 3)$ code for $e = 1.5 \times 10^{-3}$, although the use of the syndrome information smoothly widens the area. In general, the CG scenario unnecessarily smears out the qubit information kept by the measurement outcomes of intermediate stations, and thus, we find that making use of fine-grained information can be valuable. Nevertheless, the CG scenario has already shown significant performance improvement over a long distance for high coupling efficiency and low error rates [13].

The shape of the areas depends on both the block size and the error rate. Figure 12 shows the area to beat the PLOB bound for the case of the $(4, 3)$ code. An interesting feature observed in this code is that the area at a higher unit transmission grows significantly over longer distance and covers a relatively wide range of η_0 and L_{tot} , although it still requires an order of 10^{-3} physical error rate. In the case of $e = 1.0 \times 10^{-3}$, we observe a relatively slow decay of the upper end of the loop along with the line $\eta_0 = 1$, which holds over a distance of 1000 km. As we have already mentioned in Sec. II A, a better signal transmission over a long distance can be achieved when there are no channel errors by using many stations with short unit

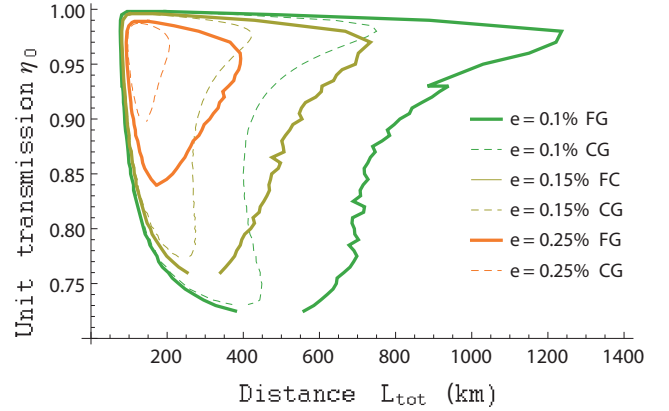


FIG. 12. Areas beating the PLOB bound for a block size of $(n, m) = (4, 3)$. Solid loops are for the FG scenario, whereas the dashed loops are for the CG scenario. The physical error rates are, respectively, $e = 1.0 \times 10^{-3}$, $e = 1.5 \times 10^{-3}$, and $e = 2.5 \times 10^{-3}$ from the largest loops to the smallest loops. A distinguishing feature is the growth of the areas toward the distance direction around $\eta_0 \sim 0.97$. This suggests that one can obtain better performance by using many intermediate stations with a short unit distance. The rightmost boundaries are jagged due to the numeric instability.

distances. This is because the loss errors can be corrected well if the distance between the stations is short. The growth and slow decay along the line $\eta_0 = 1$ here is regarded as a concrete example of such an advantage invoking the PLOB bound. The slow decay has also been observed for codes $(3, 2)$ and $(3, 3)$, although it does not reach the long distances over 1000 km (there, the longest distance to surpass the PLOB bound is achieved with a rather low unit transmission, $\eta_0 \sim 0.85$). Therefore, the graphs in Figs. 10, 11, and 12 signify the main advantage of using intermediate stations for high-rate secret key generation with relatively small block size codes.

C. Interpretation as effective quantum channels

The performance of the CG scenario can be obtained by a modification of the procedure of the intermediate stations such that they do not announce the success or failure but send vacuum states for the case of inconclusive events. With this modification the stations act as quantum channels. This constructively proves that there exists a quantum channel (completely positive trace-preserving map) which works as a repeater station; namely, a sequence of intermediate stations which works without transmission of classical information can beat the TGW bound as well as the PLOB bound. This is in sharp contrast to the no-go result for the Gaussian-channel stations [10].

IV. SUMMARY

We have analyzed potential protocols to utilize TEC one-way quantum repeater stations to increase the key rate over lossy channels beyond the fundamental bounds as given by the TGW bound and the PLOB bound. We have shown how to calculate the secret key rate of one-way intermediate stations when the syndrome information of each station is

fully available. As a general benchmark for potential quantum repeaters, we have compared the performance of the one-way scheme with the PLOB bound and numerically identified the parametric area in which our scheme surpasses the PLOB bound for a couple of small-block-size codes. We have observed that even the smallest-block-size code $(n, m) = (2, 2)$ with the CG scenario enables us to beat the PLOB bound in a middle distance, although one needs low physical errors $e \sim 10^{-4}$ and small coupling loss, such as 1%. The number of intermediate stations is typically a few hundred. In our observation, the use of syndrome information helps us to beat the PLOB bound for longer distances and enables obtaining a substantially higher secret key rate. Our results suggest that the error tolerance will be improved by using larger blocks. For instance, it has been shown that there is a substantially broad area to surpass the PLOB bound with the $(4, 3)$ code for physical errors around $e \sim 10^{-3}$. In this block size, we have observed that the distance attained by making use of the syndrome information is significantly longer than the CG scenario. In turn, the performance of the CG scenario has constructively proven the existence of a quantum channel that works as a quantum repeater. In our construction with the $(2, 2)$ code, the quantum channel acts on four photonic qubits and is regarded as an eight-mode quantum channel, while it is known [10] that Gaussian channels cannot work as quantum repeaters even if we are allowed to use arbitrarily many modes. It remains open whether the minimum number of the modes to construct an untended repeater station could be less than eight. Overall, we have observed several different aspects to highlight the potential performance of QKD with one-way intermediate stations by delving into a couple of small-block-size codes with a set of specific physical error rates. We believe our results are helpful for designing useful architecture for QKD with one-way intermediate stations in the long run.

ACKNOWLEDGMENTS

This work was supported by the DARPA Quiness program under prime Contract No. W31P4Q-12-1-0017, the NSERC Discovery Program, and Industry Canada.

APPENDIX: SUCCESS PROBABILITIES AND ERROR RATES OF A TEC STATION

In this Appendix, given a code of the TEC stations (n, m) and the error model of Sec. II B, we show how to determine the set of the success probability and logical error rates for a TEC station described in Fig. 2. See Ref. [12] further details about the TEC stations.

1. Classification of photon-loss patterns

We consider a unit of an $n \times m$ block of photonic qubits. We may call a row a subblock, which has m qubits; hence, the total number of subblocks is n . We may also use the notation (n, m) to specify the block size. In what follows, suppose that a block size (n, m) with $n, m \geq 2$ is given.

Due to the transmission loss, each qubit arrives at the next station with the probability of η_0 . Let n_{LP} denote the number of lost photons. For a block of nm photons, the probability that $n_{\text{arri}} = nm - n_{LP}$ photons arrive at the station can be

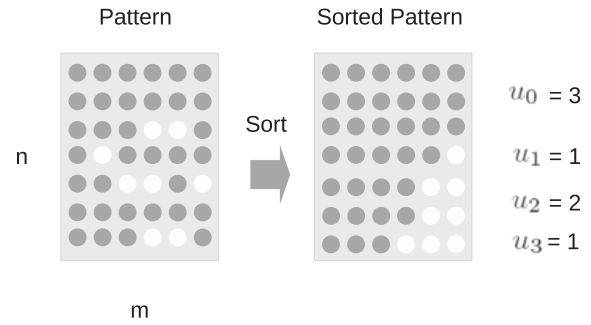


FIG. 13. Classification of patterns. The white circles indicate the position of a lost photon. For this example, the block size is $(n, m) = (7, 6)$, and the classifying index is determined to be $\vec{u} = (u_0, u_1, u_2, u_3, u_4, u_5, u_6)^T = (3, 1, 2, 1, 0, 0, 0)^T$. This implies $n_{LP} = \sum_{k=0}^{m-1} ku_k = 8$.

written as

$$p_{n_{LP}} := \text{Prob}[n_{\text{arri}} = nm - n_{LP}] = \binom{nm}{n_{LP}} \eta_0^{nm - n_{LP}} (1 - \eta_0)^{n_{LP}}. \quad (\text{A1})$$

All patterns of arriving photonic qubits can be classified by a vector $\vec{u} := (u_0, u_1, \dots, u_{m-1})^T$, where u_k represents the number of subblocks (rows) with $(m - k)$ arriving photons (see Fig. 13). We will sort a given pattern into a sorted form by moving the position of lost photons to the right side within each of subblock and shifting subblocks that have a larger number of photons upward. Then, from the sorted form we can determine the vector \vec{u} as in Fig. 13. It has to fulfill $\sum_{k=0}^{m-1} u_k = n$ and $u_0 \geq 1$ in order to satisfy that (i) at least one qubit must arrive for each subblock and (ii) at least one subblock must arrive with no loss, respectively. These conditions also imply an acceptable number of lost photons is

$$n_{LP} \leq (n - 1)(m - 1), \quad (\text{A2})$$

where the number of lost photons can be expressed in terms of \vec{u} as

$$n_{LP}(\vec{u}) = \sum_{k=0}^{m-1} ku_k. \quad (\text{A3})$$

We refer to the patterns that fulfill conditions (i) and (ii) as “acceptable” or “informative” patterns. For the informative patterns, one can basically correct loss errors and recover the logical qubit in the absence of other types of errors [12]. In practice, there are inconclusive events in which the slot is discarded even though the pattern is acceptable. We denote the rate that a sorted pattern corresponding to \vec{u} results in a conclusive event as $q_{\text{concl}|\vec{u}}$. We set $q_{\text{concl}|\vec{u}} = 0$ if \vec{u} cannot be assigned from acceptable patterns. The complete form of this rate is determined later in Eq. (A21).

Given an expression of the vector \vec{u} , any acceptable pattern can be generated from the sorted form by combining (i) a permutation of subblocks and (ii) a permutation of the photon locations within each of the subblocks. Hence, the number of possible patterns that gives a specific form of \vec{u} can be

written as

$$\begin{aligned}\Omega[\vec{u}] &:= \binom{n}{u_0, u_1, u_2, \dots, u_{m-1}} \prod_{s=1}^{m-1} \binom{m}{s}^{u_s} \\ &= \binom{n}{u_0} \prod_{s=1}^{m-1} \binom{n - \sum_{k=1}^s u_{k-1}}{u_s} \binom{m}{s}^{u_s}.\end{aligned}\quad (\text{A4})$$

Given the number of lost photons n_{LP} , the patterns associated with \vec{u} appear with the probability of

$$P_{\vec{u}|n_{LP}} = \frac{\Omega[\vec{u}]}{\binom{nm}{n_{LP}}}.\quad (\text{A5})$$

Let $E_{Z|\vec{u}}$ and $E_{X|\vec{u}}$ be the logical bit error rate and phase error rate associated with \vec{u} , respectively. The key rate for a single station can be calculated as

$$\begin{aligned}&\sum_{\vec{u}} p_{n_{LP}} q_{\text{conc}|\vec{u}} P_{\vec{u}|n_{LP}} \max[1 - h(E_{Z|\vec{u}}) - h(E_{X|\vec{u}}), 0] \\ &= \sum_{\vec{u}} q_{\text{conc}|\vec{u}} \Omega[\vec{u}] \eta_0^{nm - n_{LP}} (1 - \eta_0)^{n_{LP}} \\ &\quad \times \max[1 - h(E_{Z|\vec{u}}) - h(E_{X|\vec{u}}), 0],\end{aligned}\quad (\text{A6})$$

where we use Eqs. (A1) and (A5) and n_{LP} is given as a function of \vec{u} as in Eq. (A3). In the following part of this appendix, we show how to determine $q_{\text{conc}|\vec{u}}$, $E_{Z|\vec{u}}$, and $E_{X|\vec{u}}$.

2. The logical measurement outcomes

In the TEC process, we perform individual X measurements whose outcomes are denoted by $X_{i,j}^R$ for the incoming block R and individual Z measurements whose outcomes are denoted by $Z_{i,j}^S$ for the local block S (see Fig. 2). We set $X_{i,j} = 0$ and $Z_{i,j} = 0$ if no photon is detected at the position (i, j) in the QND measurement. The logical measurement outcomes are determined by

$$\tilde{M}_X^R = \text{sgn} \left[\sum_{i=1}^n \left(\prod_{j=1}^m X_{i,j}^R \right) \right],\quad (\text{A7})$$

$$\tilde{M}_Z^S = \prod_{i=1}^n \left[\text{sgn} \left(\sum_{j=1}^m Z_{i,j}^S \right) \right].\quad (\text{A8})$$

Here, $\text{sgn}(x)$ is associated with the majority vote and assigns $\{-1, 0, 1\}$ depending on $x < 0$, $x = 0$, or $x > 0$, respectively, while the product Π is associated with the parity. If $\tilde{M} = 0$, we discard the slot.

3. Logical X errors

According to our model in Sec. II B, each qubit of the R block suffers the phase error e_x . Hence, $X_{i,j}^R$ flips with the probability e_x . If all m qubits of i th subblock arrive, the parity of the i th subblock $\prod_{j=1}^m X_{i,j}^R$ is faithfully observed with the probability of

$$f_{X0} = \sum_{k=0}^{\lfloor \frac{m}{2} \rfloor} \binom{m}{2k} (1 - e_x)^{m-2k} e_x^{2k},\quad (\text{A9})$$

where $\lfloor \cdot \rfloor$ stands for the floor function.

Let n_M be the number of subblocks whose photons all arrived. (Only those blocks join the majority vote.) The probability that the majority vote faithfully gives the logical X is

$$F_{X|\vec{u}} = \sum_{k=0}^{\lfloor \frac{n_M-1}{2} \rfloor} \binom{n_M}{k} f_{X0}^{n_M-k} (1 - f_{X0})^k.\quad (\text{A10})$$

Recall that the number of full subblocks is specified by the first element u_0 of the vector \vec{u} . The majority vote will result in a draw with the probability of

$$D_{X|\vec{u}} = \begin{cases} \binom{n_M/2}{n_M/2} [e_x(1 - e_x)]^{n_M/2}, & n_M \text{ is even,} \\ 0, & n_M \text{ is odd.} \end{cases}\quad (\text{A11})$$

Since we discard the draw events, the success probability changes by a factor of

$$P_{\text{conc}, X|\vec{u}} := 1 - D_{X|\vec{u}}.\quad (\text{A12})$$

After discarding the draw results, the fidelity of the logical X is given by

$$F_{\text{tot}X|\vec{u}} = \frac{F_{X|\vec{u}}}{1 - D_{X|\vec{u}}}.\quad (\text{A13})$$

This implies the logical X error

$$E_{X|\vec{u}} = 1 - F_{\text{tot}X|\vec{u}} = \frac{1 - D_{X|\vec{u}} - F_{X|\vec{u}}}{1 - D_{X|\vec{u}}}.\quad (\text{A14})$$

4. Logical Z errors

According to our model in Sec. II B, each qubit of the R block suffers the bit error e_z . This implies that qubits in the position of the arriving photons of the S block suffer the same bit errors e_z due to the action of the CNOT gates. In order to determine logical Z we first execute a set of majority votes and then determine logical Z by taking the parity.

If the number of arriving photons of the i th subblock is $m_{M,i}$, the majority vote of this subblock is faithfully obtained with a probability of

$$f_{Z,i|\vec{u}} = \sum_{k=0}^{\lfloor \frac{m_{M,i}-1}{2} \rfloor} \binom{m_{M,i}}{k} (1 - e_z)^{m_{M,i}-k} e_z^k.\quad (\text{A15})$$

For each subblock, we can write the probability that the majority vote is a draw,

$$d_{Z,i|\vec{u}} = \begin{cases} \binom{m_{M,i}}{m_{M,i}/2} [e_z(1 - e_z)]^{m_{M,i}/2}, & m_{M,i} \text{ is even,} \\ 0, & m_{M,i} \text{ is odd.} \end{cases}\quad (\text{A16})$$

Like for Eq. (A10), let us define

$$F_{Z,i|\vec{u}} = \frac{f_{Z,i|\vec{u}}}{1 - d_{Z,i|\vec{u}}}.\quad (\text{A17})$$

Since we discard the draw events, the success probability changes based on the set of factors:

$$P_{\text{conc}, Z,i|\vec{u}} := 1 - d_{Z,i|\vec{u}},\quad (\text{A18})$$

where $i \in \{1, 2, \dots, n\}$.

Since we take the parity of n subblocks, the fidelity of the logical Z after discarding the draw results is given by

$$F_{\text{tot}Z|\vec{u}} = \sum_{k=0}^{\lfloor \frac{n}{2} \rfloor} \sum_{j=1}^{\binom{n}{2k}} \left[\prod_{i \in s_j^{(2k)}} (1 - F_{Z,i|\vec{u}}) \prod_{i \in \bar{s}_j^{(2k)}} F_{Z,i|\vec{u}} \right], \quad (\text{A19})$$

where $s^{(2k)} = \{s_j^{(2k)}\}_{j=1,2,\dots,\binom{n}{2k}}$ denotes the set of all possible subsets of $s_0 = \{1, 2, 3, \dots, n-1, n\}$ with the number of elements $2k$ [the length of each $s_j^{(2k)}$ is $2k$, and j runs from 1 to $\binom{n}{2k}$]. We also define $\bar{s}_j^{(2k)} = s_0 \setminus s_j^{(2k)}$. Then, the logical Z error is given by

$$E_{Z|\vec{u}} = 1 - F_{\text{tot}Z|\vec{u}}. \quad (\text{A20})$$

5. Rate for conclusive events

Using Eqs. (A12) and (A18), for any acceptable pattern associated with \vec{u} , we can assign the pair of the logical bits

(X, Z) with the rate

$$q_{\text{conc}|\vec{u}} = P_{\text{conc},X|\vec{u}} \prod_{i=1}^n P_{\text{conc},Z,i|\vec{u}}, \quad (\text{A21})$$

and we set $q_{\text{conc}|\vec{u}} = 0$ if \vec{u} is not associated with an acceptable pattern.

Now, the set of the success probability and logical error rates $\{w_i, \epsilon_i^{(z)}, \epsilon_i^{(x)}\}$ for our TEC stations is given by relabeling the index $i \rightarrow \vec{u}$ as

$$\begin{aligned} w_{\vec{u}} &= p_{n_{LP}} q_{\text{conc}|\vec{u}} P_{\vec{u}|n_{LP}}, \\ \epsilon_{\vec{u}}^{(z)} &= E_{Z|\vec{u}}, \\ \epsilon_{\vec{u}}^{(x)} &= E_{X|\vec{u}}. \end{aligned} \quad (\text{A22})$$

From this triplet, we can determine the key rate for a sequence of intermediate stations by using Eqs. (24), (25), and (26).

-
- [1] H.-J. Briegel, W. Dür, J. I. Cirac, and P. Zoller, *Phys. Rev. Lett.* **81**, 5932 (1998).
 - [2] M. Zwerger, H. Briegel, and W. Dür, *Appl. Phys. B* **122**, 1 (2016).
 - [3] K. Azuma, K. Tamaki, and H.-K. Lo, *Nat. Commun.* **6**, 6787 (2015).
 - [4] N. Sangouard, C. Simon, H. de Riedmatten, and N. Gisin, *Rev. Mod. Phys.* **83**, 33 (2011).
 - [5] M. Razavi, M. Piani, and N. Lütkenhaus, *Phys. Rev. A* **80**, 032301 (2009).
 - [6] M. Takeoka, S. Guha, and M. Wilde, *IEEE Trans. Inf. Theory* **60**, 4987 (2013).
 - [7] M. Takeoka, S. Guha, and M. M. Wilde, *Nat. Commun.* **5**, 5235 (2014).
 - [8] S. Pirandola, R. Laurenza, C. Ottaviani, and L. Banchi, [arXiv:1510.08863](https://arxiv.org/abs/1510.08863).
 - [9] R. Namiki, [arXiv:1603.05292](https://arxiv.org/abs/1603.05292).
 - [10] R. Namiki, O. Gittsovich, S. Guha, and N. Lütkenhaus, *Phys. Rev. A* **90**, 062316 (2014).
 - [11] W. Munro, A. Stephens, S. Devitt, K. Harrison, and K. Nemoto, *Nat. Photonics* **6**, 777 (2012).
 - [12] S. Muralidharan, J. Kim, N. Lütkenhaus, M. D. Lukin, and L. Jiang, *Phys. Rev. Lett.* **112**, 250501 (2014).
 - [13] S. Muralidharan, L. Li, J. Kim, N. Lütkenhaus, M. D. Lukin, and L. Jiang, *Sci. Rep.* **6**, 20463 (2016).
 - [14] W. Munro, K. Azuma, K. Tamaki, and K. Nemoto, *IEEE J. Sel. Top. Quantum Electron.* **21**, 1 (2015).
 - [15] E. Knill, R. Laflamme, and G. J. Milburn, *Nature (London)* **409**, 46 (2001).
 - [16] E. Knill, *Nature (London)* **434**, 39 (2005).
 - [17] V. Scarani, H. Bechmann-Pasquinucci, N. J. Cerf, M. Dušek, N. Lütkenhaus, and M. Peev, *Rev. Mod. Phys.* **81**, 1301 (2009).
 - [18] A. J. F. Hayes, A. Gilchrist, C. R. Myers, and T. C. Ralph, *J. Opt. B* **6**, 533 (2004).
 - [19] A. J. F. Hayes, H. L. Haselgrove, A. Gilchrist, and T. C. Ralph, *Phys. Rev. A* **82**, 022323 (2010).